The effect of group VIII elements on the magnetic and vibrational properties of MnPt alloy: ab initio study

Ramogohlo Diale[1*]*, Phuti* Ngoepe[2]*, Joseph* Moema[1]*, Hasani* Chauke[2] and *Maje* Phasha[1]

[1]Advanced Materials Division, MINTEK, South Africa
[2]Materials Modelling Centre, University of Limpopo, South Africa

Abstract. The magnetic properties of MnPt alloy have attracted much attention due to its potential use in magnetic recording and spintronics. Previous studies have indicated that this alloy retains its antiferromagnetism at room temperature. Only a few studies have been done on a ferromagnetic (FM) MnPt alloy, despite its higher magnetic moment than FePt. In this study, the effect of group VIII elements (Fe, Ru) on the thermodynamic, magnetic and vibrational properties of MnPt alloy is being investigated using density functional theory (DFT) based calculations. The heats of formation were found to increase with an increase in Fe and Ru compositions, indicating that the thermodynamic stability is not enhanced. It was also found that the ferromagnetic state is improved below 12.5 at. % Fe. The vibrational properties are estimated from the calculated phonon dispersion curves. Based on the results, these alloys would be suitable for the development of high-strength magnetic components in the future.

1 Introduction

Manganese (Mn) based intermetallic alloys represent a class of materials with a great potential in data storage applications because of their high stability as well as very high Néel temperature [1, 2]. These compounds are characterized by half-filled 3d orbitals, they exhibit an antiferromagnetic (AFM) characteristic during the formation process [2, 3]. In addition to this, other properties, such as high antiferromagnetism stability and a very high Néel temperature (TN), have also increased interest in AFM materials like MnM (M=Ni, Ir, Pd, Rh and Pt) for use in microelectronics components[2]. MnPt is the only candidate material above capable of exhibiting out-of-plane equilibrium spin texture resulting from ferromagnetic exchange interactions. Besides its high ferromagnetic (FM) stability, it also offers good exchange coupling fields. MnPt has an ordered paramagnetic cubic structure (Pm-3m), which at 970 K transforms into a tetragonal structure (CuAu-I) [4]. At 1220 K, the MnPt alloy was found to be magnetically susceptible and electrically resistant [5, 6]. In recent years, MnPt alloys have gained a lot of attention because the degree of order, the separation of atoms, and even environmental conditions can affect magnetic interactions [2, 4]. AFM active elements are commonly used in magnetic random-access memory (MRAM), but FM

---

* Corresponding author: ram@mintek.co.za

active elements made of MnPt are also used in magnetic recording and spintronic devices. In a previous study, the present authors employed density functional theory to study the influence of cobalt (Co) on properties of $Mn_{50}Pt_{50}$ alloy [7]. The researchers found that Co-inclusion enhances the magnetic properties on the Pt-sites. The same theoretical approach has also been used to examine the effect of d^{10} precious elements on the properties of $Mn_{50}Pt_{50}$ alloy [8]. Ferromagnetism was found to be maintained in the presence of Pd but lower in the presence of Au and Ag. As a result of the findings above, it appears that the Pt-site is capable of improving mechanical and magnetic properties. AFM MnPt has been the subject of most first-principles studies, but FM MnPt-X is now being studied as an effort to stabilize it in the cubic phase.

In this paper, DFT was used to examine the effect of group VIII elements (Fe and Ru) on magnetic and vibrational properties of $Mn_{50}Pt_{50-x}M_x$ ternary alloys. A study investigates the phase stability and magnetic strength of B2 MnPt phases with Fe and Ru substituted on the Pt-site.

2 Methodology

Vienna ab initio simulation package (VASP) code [9, 10] was used to perform first-principle calculations based on the density functional theory. PAW (all-electron projector augmented wave) method was used to incorporate electron and core interactions [11]. A generalized gradient approximation (GGA) [12] was applied to the exchange correlation function by Perdew, Burke and Ernzerhof (PBE) [13]. Several tests were conducted to verify convergence of the total energies with different plane-wave basis sets and k-points. A 500 eV energy cutoff was used to ensure accuracy of 1 meV per atom. As described by Monkhorst–Pack, Brillouin zone (BZ) is computed based on the use of k-point meshes with a 14x14x14 grid. The supercell consist of two 2x2x2 with 16 atoms were constructed on $Mn_{50}Pt_{50}$. In order to achieve the most stable composition, Pt was substituted with Fe and Ru using the substitutional search tool embedded in MedeA. In order to determine the ground state under different compositions, a full geometry optimization was performed. The thresholds for geometry optimization were set at a difference in total energy of within 1×10^{-6} meV/atom. A relaxation process was performed until Hellman Feynman forces decrease to less than 0.001 eV/Å. Then, thermodynamic, magnetic and vibrational properties were calculated from full optimized systems. In the MedeA software Platform, the PHONON code [14] was utilized to calculate phonon dispersion curves.

3 Results and discussion

3.1 Structural and thermodynamic properties

B2 Ferromagnetic (FM) $Mn_{50}Pt_{50}$ belong to the cubic structure with a space group Pm-3m where Mn atoms are located at the corners and Pt atoms at the face centers. FM $Mn_{50}Pt_{50}$ is approximately 2.70 Å from Mn-Pt, 3.12 Å from Mn-Mn and 3.12 Å from Pt-Pt. In order to investigate the ground-state properties of B2 $Mn_{50}Pt_{50-x}M_x$ alloys, the geometries are then optimized by fully relaxing the cell's shape and the atomic positions. In Our knowledge, experimental/theoretical values for lattice parameters (3.12 Å) of FM-B2 are not available to compare with the calculated results. Unfortunately, most of researchers have studied B2-Paramagnetic (PM) $Mn_{50}Pt_{50}$ not FM-B2 $Mn_{50}Pt_{50}$ for spintronics application which made it difficult to compare the parameters of FM. Binary B2-PM $Mn_{50}Pt_{50}$, for example, has an equilibrium lattice parameter of 3.00 Å (3.01 Å) [15], which compare well with theoretical data (in parenthesis) to 2% agreement. It suggests that the calculations in the present work

are reasonable and reliable. Considering this study is focused on FM B2 $Mn_{50}Pt_{50}$, the results presented below illustrate how Fe and Ru introduce change properties of the system.

Figure 1 (a) shows the calculated equilibrium lattice parameters of alloys as a function of M content. It can also be observed that the lattice parameters of B2 $Mn_{50}Pt_{50-x}M_x$ alloys decrease with an increase Fe and Ru content. It is a result of M's slightly smaller atomic radius than that of Pt in the Mn-Pt substitution supercell approach. Crystals' thermodynamic stability is related to their heats of formation, which are the enthalpies that change when one mole of a compound is formed from their stable states. Hence, a low heat of formation implies a high thermodynamic stability. Furthermore, the structure is easier to form in the experiment in case that the heats of formation is more negative. In the present work, the heats of formation (ΔH_f) of alloys can be obtained from the following equation:

$$\Delta H_f = E_C - \sum_i x_i E_i \tag{1}$$

where E_C is the system's calculated total energy, while E_i is the elements' calculated total energy.

The computed heats of formation are highlighted in Figure 1 (b). It can be distinguished that the calculated heats of formation of $Mn_{50}Pt_{50-x}M_x$ alloys are all negative, which shows the great possibility of forming these alloys in the experiment. In other words, higher M content reduces the thermodynamic stability of $Mn_{50}Pt_{50-x}M_x$ alloys. Although with reduced stability, $Mn_{50}Pt_{50-x}Ru_x$ is more thermodynamically favourable as compared to the $Mn_{50}Pt_{50-x}Fe_x$ above 12.50 at. % compositions.
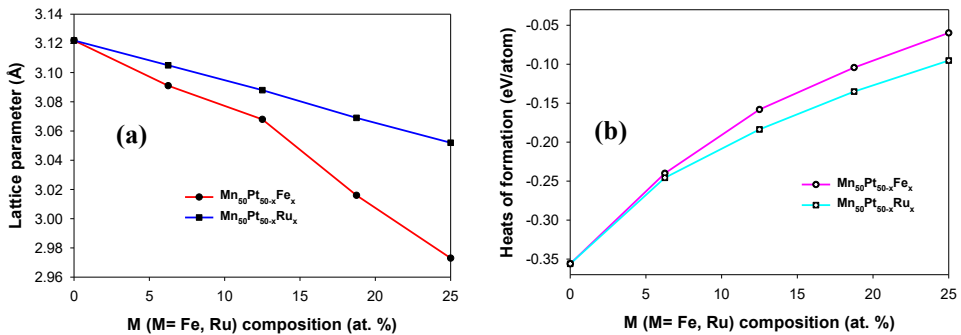

Fig. 1. (a) Equilibrium lattice parameter, a and (b) heats of formation against at. % M for B2 FM $Mn_{50}Pt_{50-x}M_x$ alloys ($0 \leq x \leq 25$).

3.2 Magnetic properties

Calculated total magnetic moments were used to measure the magnetic strength of $Mn_{50}Pt_{50-x}M_x$ systems. Positive total magnetic moments indicate strong magnetic fields. Figure 2 shows total spin magnetic moments of $Mn_{50}Pt_{50-x}M_x$ alloys. The total magnetic moment of the binary FM B2 $Mn_{50}Pt_{50}$ alloy was found to be 4.45 μ_B, unfortunately; there are no experimental data to compare. As expected, $Mn_{50}Pt_{50-x}Fe_x$ possesses the highest spin moment (below 12.5 at. % Fe) suggesting the highest magnetization on $Mn_{50}Pt_{50}$. In Figure 2, further increase in Fe (above 12.5 at.%) result in a slightly gradual reduction in magnetic moment. This suggests that the $Mn_{50}Pt_{50-x}Fe_x$ alloys are the most desirable for various magnetic applications at 12.5 at % Fe and below. Moreover, it can be seen that there is a reduction in the total magnetic moment with an increase in Ru composition, suggesting that Ru does not contribute to improving the magnetism of $Mn_{50}Pt_{50}$ alloys. Ferromagnetic element (Fe) with

smaller atomic radius (1.26 Å) showed a greater improvement than Ru with larger atomic radius (1.34 Å).
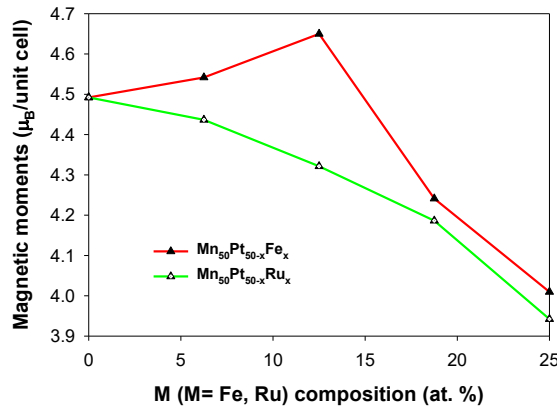

Fig. 2. Magnetic moments against composition (at. % M) for B2 $Mn_{50}Pt_{50-x}M_x$ when $0 \leq x \leq 25$ composition range.

3.3 Vibrational properties

Phonon dispersion curves play a crucial role in explaining many properties and behaviour of crystalline materials, including vibrational properties and phase transitions. Structures with no soft modes in the Brillouin zone (Bz) are considered vibrationally stable. In addition, the absence of soft modes indicates that the compound cannot undergo a martensitic phase transition, whereas a compound with soft modes can. In our other study, we found that the FM MnPt structure has no phase transition as it displayed no soft modes in the phonon dispersion curve as shown in Figure 3 (a) [8]. Now, the effect of Fe and Ru on the phonon dispersion curves of B2 $Mn_{50}Pt_{50}$ alloy is investigated and shown in Figure 3. The Phonon dispersion curves were calculated for entire compositions $0 \leq x \leq 25$ but because the systems showed similar behaviour (No soft modes), only 6.25 at. % M is shown. As the amount of Fe is added (6.25 at. % Fe), it appears that the phonon dispersion curve does not exhibits any soft modes along any of the high symmetry directions. In this case, it suggests that the structure is vibrationally stable and that there is no possibility of the structure transitioning into a lower-temperature phase. In the case of $Mn_{50}Pt_{50-x}Ru_x$ (Figure 3 (c)), it is quite evident that $Mn_{50}Pt_{43.75}Ru_{6.25}$ is vibrationally stable due to the absence of soft modes in the Brillouin zone (Bz). In this case, the addition of Ru does not result in a phase transition to lower temperature phases such as $L1_0$. According to this observation, Fe and Ru additions do not compromise B2 $Mn_{50}Pt_{50}$'s vibrational stability.
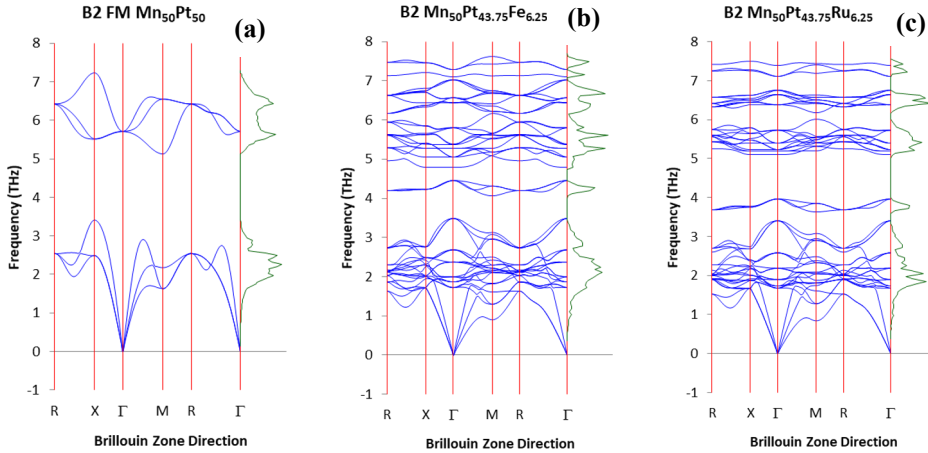
Fig. 3. The phonon dispersion curves of B2 (a) $Mn_{50}Pt_{50}$, (b) $Mn_{50}Pt_{43.75}Fe_{6.25}$ and (c) $Mn_{50}Pt_{43.75}Ru_{6.25}$ structures. The Γ (000) represents the center of the Bz.

4 Conclusion

The magnetic and vibrational properties of B2 $Mn_{50}Pt_{50-x}M_x$ alloys have been systematically investigated using DFT approach. Based on the results, Fe and Ru do not improve the thermodynamic stability of $Mn_{50}Pt_{50}$ structures, as the heats of formation increase with composition. Furthermore, the results showed that the addition of Fe below 12.5 at. % may improve the magnetism of $Mn_{50}Pt_{50}$ alloy. With Ru addition, it was also discovered that ferromagnetism was not improved. The phonon dispersion curves of B2 $Mn_{50}Pt_{50-x}M_x$ alloys showed no soft modes, indicating vibrational stability. Using the present findings as a guide, future magnetic components may be developed.

References

1. R. F. C. Farrow, R. F. Marks, S. Gider, A. C. Marley, S. S. P. Parkin, and D. Mauri, J. Appl. Phys. 81, 4986 (1997).
2. I. J. Park, T. Lee, P. Das, B. Debnath, G. P. Carman, R. K. Lake, Appl. Phys. Lett. **114**, 142403 (2019).
3. A. Sakuma, R. Y. Umetsu, K. Fukamichi, Phys. Rev. B **66**, 014432 (2002).
4. R. Y. Umetsu, K. Fukamichi and A. Sakuma, Mater. Trans. **47**, 2-10 (2006).
5. E. Krén, G. Kádár, L. Pál, J. Sólyom, P. Szabó, T. Tarnóczi, Phys. Rev. **171**, 574 (1968).
6. P. F. Ladwig, Y. A. Chang, J. Appl. Phys. **94**, 979-987 (2003).
7. R. G. Diale, P. E. Ngoepe, J. S. Moema, M. J. Phasha, H. Moller, H. R. Chauke, MRS Adv. **8**, 651-655 (2023).
8. R. Diale, P. Ngoepe, H. Chauke, J. Moema, M. Phasha, Mater. **17**, 541 (2024)

9. G. Kresse, and J. Hafner, Phys. Rev. B **47**, 58-561 (1993).

10. G. Kresse, and J. Furthmüller, Phys. Rev. B **54**, 11169-11186 (1996).

11. P. E. Blöchl, Phys. Rev. B **50**, 17953-17979 (1994).

12. J. P. Perdew, and Y. Wang, Phys. Rev. B **45**, 13244-13249 (1992).

13. J. P. Perdew, K. Burke, and M. Ernzerhof, Phys. Rev. Lett. **77**, 3865-3868 (1996).

14. K. Parlinski, Z. Q. Li and Y. Kawazoe, Phys. Rev. Lett. **78**, 4063-4066 (1997).

15. J. Wang, A. Gao, W. Chen, X. D. Zhang, B. Zhou and Z. Jiang, J. Magn. Magn. Mater. **333**, 93-99 (2013).